Longitudinal photon-momentum transfer in strong-field double ionization of argon atoms

Fenghao Sun,[1] Xiang Chen,[2] Wenbin Zhang,[1] Junjie Qiang,[1] Hui Li,[1] Peifen Lu,[1] Xiaochun Gong,[1] Qinying Ji,[1] Kang Lin,[1]
Hanxiao Li,[1] Jihong Tong,[1] Fei Chen ☉,[1] Camilo Ruiz,[3] Jian Wu,[1,4,*] and Feng He[2,†]

[1]*State Key Laboratory of Precision Spectroscopy, East China Normal University, Shanghai 200062, China*
[2]*Key Laboratory for Laser Plasmas (Ministry of Education) and School of Physics and Astronomy, Collaborative Innovation Center for IFSA*
(CICIFSA), Shanghai Jiao Tong University, Shanghai 200240, China
[3]*Instituto Universitario de Física Fundamental y Matemáticas, Universidad de Salamanca, Plaza de la Merced s/n, 37008 Salamanca, Spain*
[4]*Collaborative Innovation Center of Extreme Optics, Shanxi University, Taiyuan, Shanxi 030006, China*

We investigate the longitudinal photon-momentum transfer in nonsequential double ionization of argon atoms exposed to a 2.0-μm linearly polarized strong laser field. The zero momentum of the photoelectron is precisely calibrated using the photoelectron-photoion coincidence spectrum. The sum-longitudinal momentum of two photoelectrons from the double ionization noticeably deflects along the laser propagation direction, which is opposite to and much larger than that of single ionization. By tracking the electron trajectories for double ionization in semiclassical simulations, we find that the Coulomb focusing of the ionic core with the assistance of the Lorentz pushing of the laser field dominates the observed longitudinal momentum deflection. Our results open the possibility to control the photon-momentum transfer by manipulating the waveform of the laser fields and thus the Coulomb and magnetic effects experienced by the photoelectrons.

DOI: 10.1103/PhysRevA.101.021402

Photoionization of atoms and molecules is one of the most fundamental strong-field phenomena. It is the key to image molecular orbital structures [1–4], and to reveal the ultrafast dynamics of electron and nuclear wave packets [5–8], and has become the cornerstone in attosecond pulse characterization [9–11]. To understand the rich strong-field phenomena, the electric dipole approximation is generally adopted by assuming that the vector potential $\boldsymbol{A}$ of the laser field is spatially homogeneous [12]. As a consequence, the magnetic component of the laser field, $\boldsymbol{B} = \nabla \times \boldsymbol{A}$, and the corresponding Lorentz force $\boldsymbol{F_B} = q\boldsymbol{v} \times \boldsymbol{B}$ on the motion of the electron are neglected, where q and $\boldsymbol{v}$ are the charge and velocity of the electron. Such neglect is generally reasonable for the laser fields with moderate intensities since the magnitude of the magnetic field is much smaller than the electric field (approximately scaled by $1/c$ with c the light velocity). However, for laser fields with high intensities or long wavelengths, the magnetic field effect becomes noticeable [13], and in particular its influence on the motion of the high-velocity photoelectrons which will be deflected along the propagation direction of the laser field (denoted as the "longitudinal momentum" in this Rapid Communication). Much attention has been paid to the nondipole effects in strong-field ionization of atoms in recent years, which have been observed experimentally or theoretically for cases of various wavelengths and intensities [14–35].

For strong-field single ionization of atoms, it was recently demonstrated that the photoelectron can acquire a nonzero momentum along or against the laser propagation direction [36–39]. On the other hand, the longitudinal momentum deflections of the photoelectrons of the double ionization were numerically predicted to be much larger than that of the single ionization [40,41]. However, the corresponding nondipole effect in the *nonsequential double ionization* yet lacks experimental observation since the previous measurements were mainly performed in a velocity map imaging (VMI) apparatus without coincidence, and thereby it is hard to identify the photoelectrons from double ionization. For the nonsequential double ionization, two electrons may be released via the recollision process where the trajectories of them may be altered, leading to a nonintuitive deflection of the momentum induced by the nondipole effect.

In this Rapid Communication, we experimentally investigate the longitudinal photon-momentum transfer in strong-field nonsequential double ionization of Ar atoms by measuring the released two photoelectrons and the correlated dication in coincidence. The zero momentum is calibrated by clearly identifying the dc-field ionization of the photon excitation created Rydberg atoms in the photoelectron-photoion coincidence (PEPICO) spectrum measured in the same experiment, which is the key to precisely record the tiny deflection of the released photoelectrons. The maximal deflection of the sum-longitudinal momentum of the two photoelectrons released from the same atom via nonsequential double ionization is observed to be 0.074 ± 0.007 a.u., which is more than three times larger than that of the single ionization 0.020 ± 0.001 a.u. The deflections of the photoelectron momentum are extracted by fitting the peak of the spectrum with a Lorentzian function. Depending on the detailed trajectories as revealed in our semiclassical simulations, the photoelectrons experience different Coulomb and magnetic effects, leading to various longitudinal momentum deflections.

We performed the measurement in an ultrahigh-vacuum chamber of a cold target recoil ion momentum spectroscopy (COLTRIMS) apparatus [42,43]. The near-infrared femtosecond laser pulses (25 fs, 790 nm, and 10 kHz) from a multipass Ti:sapphire laser system were frequency down-converted to 2.0 μm by using a traveling-wave optical parametric amplifier superfluorescence system, which were afterwards focused on the supersonic gas jet of Ar atoms by a concave silver mirror ($f = 75$ mm) inside the chamber of COLTRIMS. By carefully examining the photoelectron momentum along the minor axis of the driving elliptically polarized laser fields of various ellipticities [44,45], the peak intensity of the linearly polarized laser field in the reaction region was calibrated to be 1.4×10^{14} W/cm^2 in our experiment. A double hump momentum distribution of the Ar^{2+} along the laser polarization direction is observed, indicating the dominant process of nonsequential double ionization [46,47]. The ionization-created ions and electrons guided by a weak homogenous electric field ($E_s \sim 18.5$ V/cm) and magnetic field ($B \sim 13.1$ G) are to be detected by two time- and position-sensitive microchannel plate detectors at opposite ends of the spectrometer. Three-dimensional momenta of the electrons and ions are reconstructed event by event from the measured time of flight (TOF) and positions of the charged impacts. In addition to the TOF and kinetic energy release (KER) of the correlated ions, the momentum conservation among the measured photoelectrons and ions is used to select the right events of the single and double ionization of Ar atoms. The laser propagation direction, the jet direction, and the laser polarization direction (or time-of-flight direction of the ions) are defined as the x, y, and z axes of the lab frame.

Since the deflection of the photoelectron momentum induced by the magnetic effect of the laser field is on the order of 0.01 a.u., it is critical to precisely calibrate the zero momentum. For its much longer lifetime as compared to the femtosecond temporal duration of the laser pulse, the photon-excitation created Rydberg atoms which are afterward ionized by the dc field of the spectrometer can be used to determine the zero momentum [38]. Here, different from the previous measurement using VMI [36–38] without coincidence, we purely identify the electrons released by the dc field from the Rydberg atoms using the PEPICO spectrum [48,49] to precisely determine the zero momentum. The time delay of the dc ionization of the Rydberg atoms is directly measured in the same target gas where the strong-field photoionization causes nondipole effects. All the electron-momentum distributions are obtained directly from the detected electrons. As shown in Fig. 1(a), the electrons from the dc-field ionization of the Rydberg atoms with much larger TOFs are measured as the long tail (denoted by "dc") in the PEPICO spectrum, which are clearly distinguished from the photoelectrons generated from the strong-field ionization (denoted by "laser") of the Ar atoms. The laser-excited Rydberg atom will fly tens of nanoseconds before its ionization by the dc field of the spectrometer. For a jet velocity of $vx_{\text{jet}} = 8 \times 10^{-6}$ mm/ns along the laser propagation direction owing to the imperfect geometric alignment of the experimental apparatus, the electron may obtain a momentum shift on the order of $\delta px_e \sim 0.00001$ a.u., which is much smaller than the momentum deflection induced by the laser nondipole effects and thus
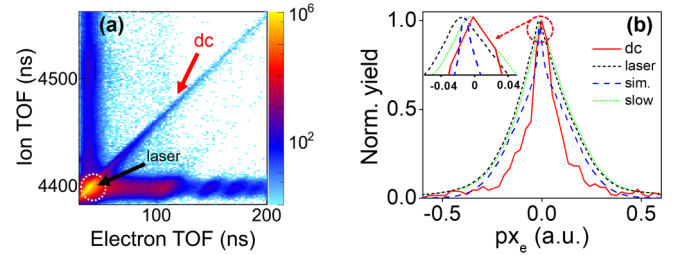

FIG. 1. (a) Measured photoelectron-photoion coincidence spectrum and (b) longitudinal momentum spectra of electrons released by the dc field (dc, red solid curve), the strong laser field (laser, black short-dashed curve) together with the numerically simulated one (sim., blue dashed curve), and the slow electrons (slow, green dotted curve), for the single ionization of Ar atoms.

can be neglected. The electron spectrum obtained by cutting the central area of the electron momentum distribution [36] is also shown in Fig. 1(b) as a reference, which is denoted as the "slow" electrons in the following discussion. However, the slow electrons shown in Fig. 1(b) are mixed with the photoelectrons from the strong-field ionization and electrons from the dc-field ionization. As plotted in Fig. 1(b), the electron spectrum of the Rydberg ionization (red solid curve) identified using the PEPICO spectrum is sharper than that by merely selecting all the slow electrons (green dotted curve). The extracted electrons from the dc-field ionization of the Rydberg atoms routinely avoid the influences of the electric and magnetic fields of the laser pulse, which allows us to precisely determine the zero momentum of the photoelectron spectrum along the laser propagation direction.

To assure the feasibility of this strategy, we present the longitudinal momentum distribution of the photoelectrons from the single ionization of Ar in Fig. 1(b) (black short-dashed curve), which deflects to the opposite direction of the laser propagation by $\delta px_e \sim -0.020 \pm 0.001$ a.u. This observation coincides with previous measurements using a VMI spectrometer [36–38] and our numerical simulations [blue dashed curve in Fig. 1(b); see the description of the simulation method below], which thus confirms the validity of our strategy. We note that the longitudinal photon-momentum transfer in strong-field single ionization of atoms, in particular its partition between the ejected photoelectron and ion [34,35], was very recently experimentally examined [50]. As compared to the single ionization, here we are focusing on the photon-momentum transfer in strong-field nonsequential double ionization of atoms as detailed in the following.

The coincident measurement of two photoelectrons with the correlated dication and the momentum conservation among them allows us to identify the right events of double ionization from those of the single ionization. As shown in Fig. 2(a) (blue dashed curve), the peak of the sum momentum of two photoelectrons of doubly ionized Ar atoms along the laser propagation direction, i.e., $px_{e1} + px_{e2}$, is measured to be deflected to $\delta px_e \sim 0.053 \pm 0.004$ a.u., which is much larger than that of the single ionization as theoretically predicted [40,41]. Here, we provide an experimental observation of the longitudinal photoelectron momentum deflection along the
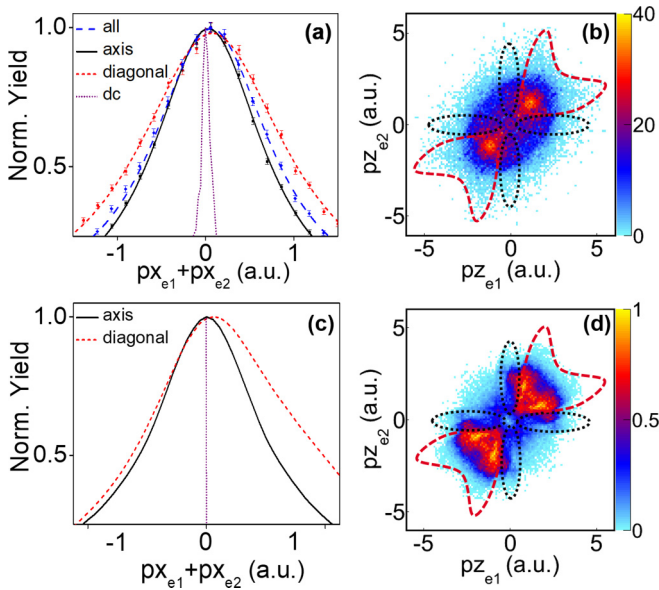
FIG. 2. (a) Measured sum-momentum spectrum of two photo-electrons (blue dashed curve), and the spectra correlated to the diagonal (red short-dashed curve) and near-axis (black solid curve) events, and (b) the photoelectron-photoelectron momentum spectrum of doubly ionized Ar atoms. (c) Simulated photoelectron sum-momentum spectra correlated to the diagonal (red short-dashed curve) and near-axis (black solid curve) events, and (d) the yield-normalized photoelectron-photoelectron momentum spectrum. The areas within red dashed lines depict the diagonal events and those within black short-dashed ellipses stand for the near-axis events. The spectrum of electrons released by the dc-field ionization of the Rydberg atoms is also plotted in (a).

laser propagation direction in strong-field double ionization of atoms.

Depending on the releasing order of two photoelectrons, the strong-field double ionization occurs either sequentially or nonsequentially. Different from the sequential double ionization, in the nonsequential double ionization the releasing processes of the two photoelectrons are correlated. Due to the periodical oscillation of the laser fields and the attractive Coulomb potential of the ionic core, the preliberated electron may be driven back and recollide with the parent core, leading to the emission of the second electron [51]. In this case, the trajectories of the two electrons sensitively rely on the recollision details (e.g., rescattering time, momentum, laser waveform). Ultimately, photoelectrons undergoing different trajectories will show up in distinct regions in their correlated momentum spectrum, which allows us to experimentally investigate the trajectory-dependent nondipole effects in nonsequential double ionization of atoms.

Figure 2(b) displays the measured photoelectron-photoelectron momentum spectrum of two correlated photoelectrons of doubly ionized Ar atoms, which has been symmetrized by exchanging the indices of the two detected electrons similar to previous measurements since the detector cannot distinguish the first and second electrons [52]. As shown in Fig. 2(a), the sum longitudinal momenta of two released photoelectrons are deflected by $\delta px_e \sim 0.036 \pm 0.007$ a.u. and 0.074 ± 0.007 a.u., respectively, for the

near-axis (within black short-dashed ellipses) and diagonal (within red dashed lines) events. The underlying physics of the trajectory-dependent nondipole effects can be revealed in our semiclassical simulations. As shown in Figs. 2(d) and 2(c), the simulated correlated photoelectron momentum spectra and the corresponding sum-longitudinal-momentum distributions of two photoelectrons of the diagonal and near-axis events agree well with the experimental observations.

In our semiclassical simulations, one electron is tunneling ionized in the strong laser field and the tunneling process is described by the Ammosov-Delone-Krainov model [53]. In the tunneling process, the electron momentum in the propagation direction acquires an upward shift of $0.3I_{p1}/c$ caused by the magnetic field [34], where $I_{p1} = 0.58$ a.u. is the first ionization energy of Ar atoms and c is the light velocity. Therefore, the initial momentum distribution of the tunneling electron is formulated as $W(vx, vy) = \frac{2(2I_{p1})^{1/2}}{|E(t)|}\exp\{-\frac{[(vx-0.3I_{p1}/c)^2+vy^2](2I_{p1})^{1/2}}{|E(t)|}\}$, where vx and vy are the electron initial velocities orthogonal to the laser polarization direction z, and $vz = 0$ by assuming the adiabatic tunneling ionization. The subsequent propagation of the tunneling ionized electron as well as the motion of the second electron after its release upon the recollision is governed by the Newtonian equation, which can be expressed as $\frac{d^2 r_i}{dt^2} = -\nabla_{r_i}(V_{ne}^i + V_{ee}) + qE(t) + q\frac{dr_i}{dt} \times B(t)$, where $V_{ne}^i = -\frac{2}{\sqrt{r_i^2+a}}$ is Coulomb interactions between a nucleus and electrons, and $V_{ee} = \frac{1}{\sqrt{(r_1-r_2)^2+a}}$ is Coulomb interactions between two electrons. Here the soft core parameter $a = 0.1$ is used to remove the singularity of the Coulomb potential. The equation is solved by using the Runge-Kutta algorithm and the laser electric field and magnetic field are both included in calculations. We notice that Emmanouilidou [41] dealt with the singularity of the Coulomb potential by regularizing the electron coordinates. Totally, more than one million double ionization events are collected. The convergence is achieved after setting the relative error and absolute error as 10^{-8} and 10^{-9} in calculations. The electric field of the linearly polarized laser pulse is expressed as $E(t) = f(t)E_0 \cos(\omega t)\hat{e}_z$ and the magnetic field is given as $B(t) = \hat{e}_x \times E(t)/c$, where $f(t)$ denotes the pulse envelope with two cycles plateau followed by one cycle ramp off; the E_0 and ω are the electric field amplitude and frequency of the driving laser pulse, respectively; $\hat{e}_z$ and $\hat{e}_x$ are the unit vector in the z and x directions. The laser intensity and wavelength are the same as those used in our experiment.

By tracking the time evolution of electron trajectories, one may extract the instants for tunneling (T_{ti}), recollision (T_{rc}), and double ionization (T_{di}). Here, T_{ti} is the instant when the first electron tunnels out of the laser-dressed Coulomb potential of the ionic core, T_{rc} is the instant that the electron moves nearest to its parent ion after the tunneling, and T_{di} is the instant that the sum of potential and kinetic energies for each electron becomes positive. The rescattering mostly occurs around the zero crossing of the electric field or the maximum of the vector potential of the laser pulse. Recollision-induced double ionization events can be divided into two groups, i.e., the first return as $\Delta T = T_{rc} - T_{ti} < 1\,T$ and the second return as $1\,T < \Delta T < 1.5\,T$. In Figs. 3(a) and 3(b), we grouped
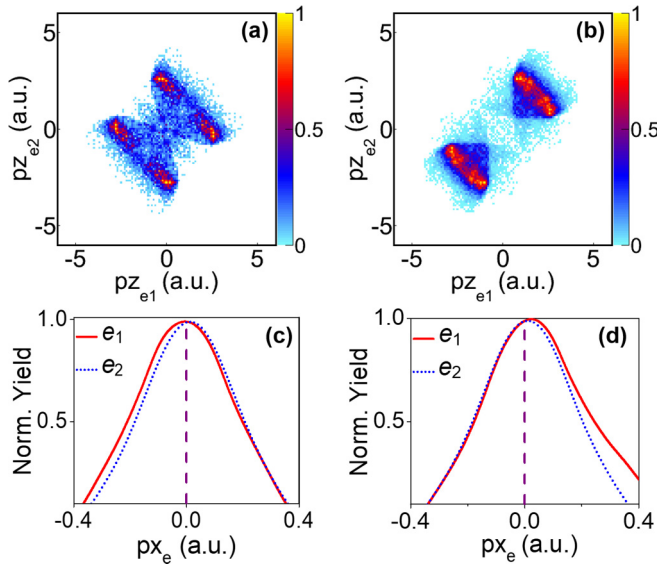
FIG. 3. Simulated photoelectron-photoelectron momentum spectra of the double ionization when electron recollision happens at (a) the first return and (b) the second return. The longitudinal momentum distributions for the first tunneled electron e_1 (red solid curve) and the second impact-released electron e_2 (blue dotted curve) according to (c) the first return and (d) the second return, respectively.
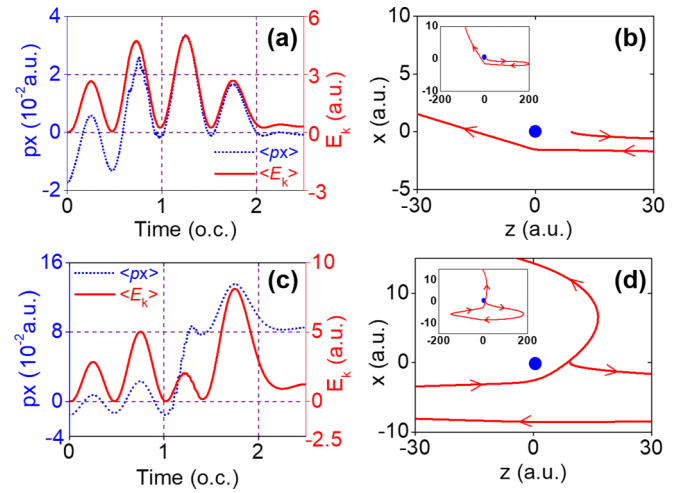

FIG. 4. The time evolution of the averaged longitudinal momentum $\langle px \rangle$ (blue dotted curve, left vertical axis) and the kinetic energy $\langle E_k \rangle$ (red solid curve, right vertical axis) of e_1 for (a) the first return and (c) the second return electron. The typical trajectories of e_1 for (b) the first return and (d) the second return, where the blue dots represent the ionic cores.

the events produced by the electron recollision at the first and second returns, respectively, which correspond to the near-axis and diagonal events in Fig. 2(d). For recollision occurring at the first return, the rescattering electron e_1 carries the kinetic momentum up to $1.26A_0$ [54], where A_0 is the amplitude of the laser vector potential. For the 2.0-μm laser pulse with a peak intensity of 1.4×10^{14} W/cm^2, this rescattering energy is much larger than the threshold for kicking out the second electron from Ar$^+$ (second ionization potential $I_{p2} = 1$ a.u.) directly, as shown by the time-dependent averaged energy of e_1 (red solid curve) in Fig. 4(a). Consequently, the rescattering electron e_1 only needs to share a little energy with the other electron e_2 to get it free, and the reserved momentum is about $1.1A_0$. The rescattering electron e_1 reserves the most energy just after the rescattering around $t = 0.75\ T$ and is decelerated by the remaining laser field; meanwhile the newly freed electron e_2 with little initial energy is accelerated by the remaining laser field. Ultimately, the first tunneling electron e_1 ends with little energy and the second freed electron e_2 gains high energy, and the corresponding double ionization events are registered near the axis of their correlated momentum spectrum as shown in Fig. 3(a). On the contrary, when the rescattering process happens at the second return around $t = 1.25\ T$, the rescattering electron e_1 carries the low energy which is just sufficient to kick out the second electron e_2, as shown by the time-dependent averaged energy of e_1 in Fig. 4(c). Therefore, after the rescattering, both electrons have very low kinetic energy and are drifted by the remaining laser field, ending with similar momenta and registering along the diagonal of their correlated momentum spectrum as shown in Fig. 3(b).

Both experimentally observed and numerically simulated results show that the sum-momentum deflection of two

photoelectrons in the laser propagation direction of the near-axis events is smaller than that of the diagonal events. To explore the underlying mechanism, we decouple the sum longitudinal momentum shown in Fig. 2(c) into the individual electron longitudinal momentum, as shown in Figs. 3(c) and 3(d) for the near-axis and diagonal events, respectively. The longitudinal momentum distributions of the secondly freed electron (e_2, blue dotted curves) in Figs. 3(c) and 3(d) have similar profiles and both peaks shift by 0.021 a.u., which are within expectation since in both cases the dynamics of this secondly freed electron is similarly driven by the oscillating laser field. However, the longitudinal momentum spectra of e_1 (red solid curves) in Figs. 3(c) and 3(d) are distinct, as are the two curves for e_1 and e_2 in Fig. 3(d).

The two very distinct curves in Fig. 3(d) indicate that the electron e_1 tunneled just after $t = 0$ acquires a large longitudinal momentum shift at the second return around $t = 1.25\ T$ since both electrons behave analogously after the double ionization. Such a statement is supported by the mean values of the time-dependent px of e_1 (blue dotted curve) shown in Figs. 4(a) and 4(c) for the first and second returns, respectively. Because of the magnetic field, the symmetry of the electron movement along the laser propagation direction is broken, and thus only the electron e_1 with negative px at tunneling is able to hit the parent ion at around either $t = 0.75\ T$ or $1.25\ T$. Therefore, one may clearly see that the px of e_1 at the starting points in Figs. 4(a) and 4(c) are both negative. The magnetic force exerting on the electron oscillates with a doubled frequency of the driving laser field, which determines the evolution of the time-dependent longitudinal momentum. At the instant of the second return, the longitudinal momentum of e_1 increases quickly. The quick increasing of px of e_1 in Fig. 4(c) and the difference of two returns can be understood by looking into the typical electron trajectories of e_1 for the first and second returns presented in Figs. 4(b) and 4(d). Because of the initially negative px of e_1 at tunneling, this

electron moves in the space $x < 0$ before rescattering. For the first return, the tunneled electron e_1 rescatters with the parent ion with the energy as large as 4.5 a.u., and thus the Coulomb field does not have enough time to deflect such a quickly moving electron. In this case, the Coulomb field contributes a small px shift, and the finally observed px shift is mainly induced by the Lorentz force. However, for the second return, the electron e_1 passes through the nuclei two times [e.g., $x = -8$ and -2 a.u. with the energy 5.62 and 1.37 a.u. for the typical trajectory shown in Fig. 4(d)]. Therefore, the Coulomb field of ionic core acts on the electron e_1 quite a long time and gives a distinct impact along the $+x$ direction, explaining the rapid increase of px shown in Fig. 4(b) at the second return. We emphasize that there would be no px deflection if there is no magnetic field action though the Coulomb field always acts on the rescattering electron.

In summary, we experimentally observed photon-momentum transfer along the laser propagation direction in strong-field double ionization of Ar atoms. The deflection of the longitudinal sum momentum of two photoelectrons caused by the magnetic effect and Coulomb bending is experimentally observed in the strong-field double ionization of atoms. The amount of longitudinal photon-momentum transfer in the nonsequential double ionization critically depends on the detailed trajectories of the released photoelectrons. Upon the recollision, the first electron shares its kinetic energy with the second electron in different manners and leads to different photon-momentum transfer to the two photoelectrons. Looking forward into the future, by manipulating the waveform of the laser field, one may precisely control the motion of the photoelectrons and the nondipole effects, leading to controllable photon-momentum transfer in the strong-field ionization of atoms and molecules.

[1] M. Meckel, D. Comtois, D. Zeidler, A. Staudte, D. Pavičić, H. C. Bandulet, H. Pépin, J. C. Kieffer, R. Dörner, D. M. Villeneuve, and P. B. Corkum, Science **320**, 1478 (2008).

[2] D. Pavičić, K. F. Lee, D. M. Rayner, P. B. Corkum, and D. M. Villeneuve, Phys. Rev. Lett. **98**, 243001 (2007).

[3] J. Wu, M. Kunitski, L. P. H. Schmidt, T. Jahnke, and R. Dörner, J. Chem. Phys. **137**, 104308 (2012).

[4] J. Voigtsberger, S. Zeller, J. Becht, N. Neumann, F. Sturm, H.-K. Kim, M. Waitz, F. Trinter, M. Kunitski, A. Kalinin, J. Wu, W. Schöllkopf, D. Bressanini, A. Czasch, J. B. Williams, K. Ullmann-Pfleger, L. P. H. Schmidt, M. S. Schöffler, R. E. Grisenti, T. Jahnke, and R. Dörner, Nat. Commun. **5**, 5765 (2014).

[5] H. Niikura, F. Légaré, R. Hasbani, M. Y. Ivanov, D. M. Villeneuve, and P. B. Corkum, Nature (London) **421**, 826 (2003).

[6] M. Odenweller, N. Takemoto, A. Vredenborg, K. Cole, K. Pahl, J. Titze, L. P. H. Schmidt, T. Jahnke, R. Dörner, and A. Becker, Phys. Rev. Lett. **107**, 143004 (2011).

[7] C. I. Blaga, J. L. Xu, A. D. DiChiara, E. Sistrunk, K. K. Zhang, P. Agostini, T. A. Miller, L. F. DiMauro, and C. D. Lin, Nature (London) **483**, 194 (2012).

[8] M. Kübel, Z. Dube, A. Yu. Naumov, D. M. Villeneuve, P. B. Corkum, and A. Staudte, Nat. Commun. **10**, 1042 (2019).

[9] M. Ferray, A. L' Huillier, X. F. Li, L. A. Lompré, G. Mainfray, and C. Manus, J. Phys. B **21**, L31 (1988).

[10] G. Sansone, E. Benedetti, F. Calegari, C. Vozzi, L. Avaldi, R. Flammini, L. Poletto, P. Villoresi, C. Altucci, R. Velotta, S. Stagira, S. De Silvestri, and M. Nisoli, Science **314**, 443 (2006).

[11] K. Zhao, Q. Zhang, M. Chini, Y. Wu, X. W. Wang, and Z. H. Chang, Opt. Lett. **37**, 3891 (2012).

[12] D. B. Milošević, G. G. Paulus, D. Bauer, and W. Becker, J. Phys. B **39**, R203 (2006).

[13] H. R. Reiss, Phys. Rev. Lett. **101**, 043002 (2008).

[14] P. L. He, D. Lao, and F. He, Phys. Rev. Lett. **118**, 163203 (2017).

[15] C. I. Moore, J. P. Knauer, and D. D. Meyerhofer, Phys. Rev. Lett. **74**, 2439 (1995).

[16] M. W. Walser, C. H. Keitel, A. Scrinzi, and T. Brabec, Phys. Rev. Lett. **85**, 5082 (2000).

[17] C. C. Chirilă, N. J. Kylstra, R. M. Potvliege, and C. J. Joachain, Phys. Rev. A **66**, 063411 (2002).

[18] S. Palaniyappan, A. DiChiara, E. Chowdhury, A. Falkowski, G. Ongadi, E. L. Huskins, and B. C.Walker, Phys. Rev. Lett. **94**, 243003 (2005).

[19] M. Førre, J. P. Hansen, L. Kocbach, S. Selstø, and L. B. Madsen, Phys. Rev. Lett. **97**, 043601 (2006).

[20] M. Klaiber, K. Z. Hatsagortsyan, and C. H. Keitel, Phys. Rev. A **74**, 051803(R) (2006).

[21] A. S. Titi and G.W. F. Drake, Phys. Rev. A **85**, 041404(R) (2012).

[22] I. A. Ivanov, Phys. Rev. A **91**, 043410 (2015).

[23] M. X. Wang, H. Liang, X. R. Xiao, S. G. Chen, W. C. Jiang, and L. Y. Peng, Phys. Rev. A **98**, 023412 (2018).

[24] N. J. Kylstra, R. A. Worthington, A. Patel, P. L. Knight, J. R. Vázquez de Aldana, and L. Roso, Phys. Rev. Lett. **85**, 1835 (2000).

[25] M. Y. Emelin and M. Y. Ryabikin, Phys. Rev. A **89**, 013418 (2014).

[26] A. Staudt and C. H. Keitel, Phys. Rev. A **73**, 043412 (2006).

[27] B. Krässig, M. Jung, D. S. Gemmell, E. P. Kanter, T. LeBrun, S. H. Southworth, and L. Young, Phys. Rev. Lett. **75**, 4736 (1995).

[28] N. L. S. Martin, D. B. Thompson, R. P. Bauman, C. D. Caldwell, M. O. Krause, S. P. Frigo, and M. Wilson, Phys. Rev. Lett. **81**, 1199 (1998).

[29] V. K. Dolmatov and S. T. Manson, Phys. Rev. Lett. **83**, 939 (1999).

[30] O. Hemmers, R. Guillemin, D. Rolles, A. Wolska, D. W. Lindle, E. P. Kanter, B. Krässig, S. H. Southworth, R. Wehlitz, B. Zimmermann, V. McKoy, and P. W. Langhoff, Phys. Rev. Lett. **97**, 103006 (2006).

[31] J. Liu, Q. Z. Xia, J. F. Tao, and L. B. Fu, Phys. Rev. A **87**, 041403(R) (2013).

[32] J. F. Tao, Q. Z. Xia, J. Cai, L. B. Fu, and J. Liu, Phys. Rev. A **95**, 011402(R) (2017).

[33] S. Chelkowski and A. D. Bandrauk, Phys. Rev. A **97**, 053401 (2018).

[34] S. Chelkowski, A. D. Bandrauk, and P. B. Corkum, Phys. Rev. Lett. **113**, 263005 (2014).

[35] S. Chelkowski, A. D. Bandrauk, and P. B. Corkum, Phys. Rev. A **95**, 053402 (2017).

[36] A. Ludwig, J. Maurer, B. W. Mayer, C. R. Phillips, L. Gallmann, and U. Keller, Phys. Rev. Lett. **113**, 243001 (2014).

[37] J. Daněk, M. Klaiber, K. Z. Hatsagortsyan, C. H. Keitel, B. Willenberg, J. Maurer, B. W. Mayer, C. R. Phillips, L. Gallmann, and U. Keller, J. Phys. B: At., Mol. Opt. Phys. **51**, 114001 (2018).

[38] C. T. L. Smeenk, L. Arissian, B. Zhou, A. Mysyrowicz, D. M. Villeneuve, A. Staudte, and P. B. Corkum, Phys. Rev. Lett. **106**, 193002 (2011).

[39] N. Haram, I. Ivanov, H. Xu, K. T. Kim, A. Atia-tul-Noor, U. S. Sainadh, R. D. Glover, D. Chetty, I. V. Litvinyuk, and R. T. Sang, Phys. Rev. Lett. **123**, 093201 (2019).

[40] A. Emmanouilidou, T. Meltzer, and P. B. Corkum, J. Phys. B: At., Mol. Opt. Phys. **50**, 225602 (2017).

[41] A. Emmanouilidou and T. Meltzer, Phys. Rev. A **95**, 033405 (2017).

[42] R. Dörner, V. Mergel, O. Jagutzki, L. Spielberger, J. Ullrich, R. Moshammer, and H. Schmidt-Böcking, Phys. Rep. **330**, 95 (2000).

[43] J. Ullrich, R. Moshammer, A. Dorn, R. Dörner, L. P. H. Schmidt, and H. Schmidt-Böcking, Rep. Prog. Phys. **66**, 1463 (2003).

[44] W. Zhang, Z. Yu, X. Gong, J. Wang, P. Lu, H. Li, Q. Song, Q. Ji, K. Lin, J. Ma, H. Li, F. Sun, J. Qiang, H. Zeng, F. He, and J. Wu, Phys. Rev. Lett. **119**, 253202 (2017).

[45] A. S. Landsman, C. Hofmann, A. N. Pfeiffer, C. Cirelli, and U. Keller, Phys. Rev. Lett. **111**, 263001 (2013).

[46] R. Moshammer, B. Feuerstein, W. Schmitt, A. Dorn, C. D. Schröter, J. Ullrich, H. Rottke, C. Trump, M. Wittmann, G. Korn, K. Hoffmann, and W. Sandner, Phys. Rev. Lett. **84**, 447 (2000).

[47] B. Wolter, M. G. Pullen, M. Baudisch, M. Sclafani, M. Hemmer, A. Senftleben, C. D. Schröter, J. Ullrich, R. Moshammer, and J. Biegert, Phys. Rev. X **5**, 021034 (2015).

[48] S. Larimian, S. Erattupuzha, C. Lemell, S. Yoshida, S. Nagele, R. Maurer, A. Baltuška, J. Burgdörfer, M. Kitzler, and X. H. Xie, Phys. Rev. A **94**, 033401 (2016).

[49] J. Ma, H. Li, K. Lin, Q. Ji, W. Zhang, H. Li, F. Sun, J. Qiang, P. Lu, X. Gong, and J. Wu, Phys. Rev. A **99**, 023414 (2019).

[50] A. Hartung, S. Eckart, S. Brennecke, J. Rist, D. Trabert, K. Fehre, M. Richter, H. Sann, S. Zeller, K. Henrichs, G. Kastirke, J. Hoehl, A. Kalinin, M. S. Schöffler, T. Jahnke, L. P. H. Schmidt, M. Lein, M. Kunitski, and R. Dörner, Nat. Phys. **15**, 1222 (2019).

[51] P. B. Corkum, Phys. Rev. Lett. **71**, 1994 (1993).

[52] A. Staudte, C. Ruiz, M. Schöffler, S. Schössler, D. Zeidler, T. Weber, M. Meckel, D. M. Villeneuve, P. B. Corkum, A. Becker, and R. Dörner, Phys. Rev. Lett. **99**, 263002 (2007).

[53] M. V. Ammosov, N. B. Delone, and V. P. Krainov, Sov. Phys. JETP **64**, 1191 (1986).

[54] Z. J. Chen, A. T. Le, T. Morishita, and C. D. Lin, Phys. Rev. A **79**, 033409 (2009).